J|A|C|S ARTICLES

Published on Web 06/15/2010

Probing the Surface of Transition-Metal Nanocrystals by Chemiluminesence

Galyna Krylova,[†] Nada M. Dimitrijevic,[†,‡] Dmitri V. Talapin,[†,§] Jeffrey R. Guest,[†] Holger Borchert,[||] Arun Lobo,[⊥] Tijana Rajh,[†] and Elena V. Shevchenko*[,†]

Center for Nanoscale Materials, Argonne National Laboratory, Argonne, Illinois 60439, Chemical Sciences and Engineering Division, Argonne National Laboratory, Argonne, Illinois 60439, Department of Chemistry, University of Chicago, Chicago, Illinois 60637, Energy and Semiconductor Research laboratory, Department of Physics, University of Oldenburg, Oldenburg, 26111, Germany, and HASYLAB at DESY, Hamburg, D-22607, Germany

Received March 23, 2010; E-mail: eshevchenko@anl.gov

Abstract: We propose a simple chemiluminescence (CL) method for investigation of the surface of Co-based nanocrystals (NCs). Using a combination of CL and spin-trap electron paramagnetic resonance techniques, we systematically studied the generation of reactive oxygen species (ROS) at the surface of differently sized $CoPt_3$ spherical NCs and $CoPt_3$/Au nanodumbbells. We have shown that differently sized $CoPt_3$ NCs can promote the formation of ROS and as a result can lead to the oxidation of luminol accompanied by the emission of the light. CL allows monitoring the stability of transition-metal-based NCs against oxidation and dissolution. We found by CL that cobalt ions slowly leach from the surface of $CoPt_3$ NCs even under very mild conditions; however, the amount of the leached cobalt ions does not exceed the maximal concentration of cobalt at the NC surface indicating that only surface atoms can go into solution.

Introduction

Transition-metal-based nanocrystals (NCs) are of great interest because of their interesting magnetic,[1,2] magnetoelectronic,[3−5] and catalytic properties.[6,7] They are also very promising for biomedical applications in cancer treatment.[8,9] Alloys of Pt with 3d transition metals have demonstrated high catalytic activity in the oxygen reduction[10−13] that is very important for further improvement of fuel cells.

Recent progress in colloidal synthesis provided access to many types of materials in the form of monodisperse particles with precisely controlled size, shape, structure, and composition.[14−18] Due to their small size, the surface of NCs plays a substantial role in the properties of NCs. Some of the application areas are extremely sensitive to the electronic states and composition of the surface of NCs. For example, the electronic structure and chemical composition of the inorganic core and organic shell affect the ability of NC to serve as a seed material for the growth of complex multicomponent systems such as binary NCs of $FePt/Fe_xO_y$,[19] $CoPt_3$/Au,[20] and FePt/CdS[21] and Fe_xO_y NCs

[†] Center for Nanoscale Materials, Argonne National Laboratory.
[‡] Chemical Sciences and Engineering Division, Argonne National Laboratory.
[§] Department of Chemistry, University of Chicago.
[||] Department of Physics, University of Oldenburg.
[⊥] HASYLAB at DESY.

(1) Lacroix, L. M.; Malaki, R. B.; Carrey, J.; Lachaize, S.; Respaud, M.; Goya, G. F.; Chaudret, B. *J. Appl. Phys.* **2009**, *105*, 023911.
(2) Zafiropoulou, I.; Devlin, E.; Boukos, N.; Niarchos, D.; Petridis, D.; Tzitzios, V. *Chem. Mater.* **2007**, *19*, 1898–1900.
(3) Liu, C.; Wu, X. W.; Klemmer, T.; Shukla, N.; Weller, D. *Chem. Mater.* **2005**, *17*, 620–625.
(4) Salgueirino-Maceira, V.; Liz-Marzan, L. M.; Farle, M. *Langmuir* **2004**, *20*, 6946–6950.
(5) Sun, S. H.; Anders, S.; Thomson, T.; Baglin, J. E. E.; Toney, M. F.; Hamann, H. F.; Murray, C. B.; Terris, B. D. *J. Phys. Chem. B* **2003**, *107*, 5419–5425.
(6) Chen, W.; Kim, J. M.; Xu, L. P.; Sun, S. H.; Chen, S. W. *J. Phys. Chem. C* **2007**, *111*, 13452–13459.
(7) Jacinto, M. J.; Kiyohara, P. K.; Masunaga, S. H.; Jardim, R. F.; Rossi, L. M. *Appl. Catal. A: Gen.* **2008**, *338*, 52–57.
(8) Choi, J. S.; Choi, H. J.; Jung, D. C.; Lee, J. H.; Cheon, J. *Chem. Commun.* **2008**, 2197–2199.
(9) Xu, C. J.; Yuan, Z. L.; Kohler, N.; Kim, J. M.; Chung, M. A.; Sun, S. H. *J. Am. Chem. Soc.* **2009**, *131*, 15346–15351.
(10) Yang, H.; Alonso-Vante, N.; Lamy, C.; Akins, D. L. *J. Electrochem. Soc.* **2005**, *152*, A704–A709.
(11) Stamenkovic, V. R.; Mun, B. S.; Arenz, M.; Mayrhofer, K. J. J.; Lucas, C. A.; Wang, G. F.; Ross, P. N.; Markovic, N. M. *Nat. Mater.* **2007**, *6*, 241–247.
(12) Chen, W.; Kim, J. M.; Sun, S. H.; Chen, S. W. *J. Phys. Chem. C* **2008**, *112*, 3891–3898.
(13) Wang, C.; van der Vilet, D.; Chang, K. C.; You, H. D.; Strmcnik, D.; Schlueter, J. A.; Markovic, N. M.; Stamenkovic, V. R. *J. Phys. Chem. C* **2009**, *113*, 19365–19368.
(14) Murray, C. B.; Sun, S. H.; Doyle, H.; Betley, T. *MRS Bull.* **2001**, *26*, 985–991.
(15) Shevchenko, E. V.; Talapin, D. V.; Rogach, A. L.; Kornowski, A.; Haase, M.; Weller, H. *J. Am. Chem. Soc.* **2002**, *124*, 11480–11485.
(16) Redl, F. X.; Black, C. T.; Papaefthymiou, G. C.; Sandstrom, R. L.; Yin, M.; Zeng, H.; Murray, C. B.; O'Brien, S. P. *J. Am. Chem. Soc.* **2004**, *126*, 14583–14599.
(17) Nandwana, V.; Elkins, K. E.; Poudyal, N.; Chaubey, G. S.; Yano, K.; Liu, J. P. *J. Phys. Chem. C* **2007**, *111*, 4185–4189.
(18) Monnier, V.; Delalande, M.; Bayle-Guillemaud, P.; Samson, Y.; Reiss, P. *Small* **2008**, *4*, 1139–1142.
(19) Figuerola, A.; Fiore, A.; Di Corato, R.; Falqui, A.; Giannini, C.; Micotti, E.; Lascialfari, A.; Corti, M.; Cingolani, R.; Pellegrino, T.; Cozzoli, P. D.; Manna, L. *J. Am. Chem. Soc.* **2008**, *130*, 1477–1487.
(20) Pellegrino, T.; Fiore, A.; Carlino, E.; Giannini, C.; Cozzoli, P. D.; Ciccarella, G.; Respaud, M.; Palmirotta, L.; Cingolani, R.; Manna, L. *J. Am. Chem. Soc.* **2006**, *128*, 6690–6698.
(21) Gu, H. W.; Zheng, R. K.; Zhang, X. X.; Xu, B. *J. Am. Chem. Soc.* **2004**, *126*, 5664–5665.

 10.1021/ja102413k

decorated with two differently sized Au NCs ($Fe_xO_y/Au_1/Au_2$).[22] These transition-metal-based NCs have demonstrated enhanced electrocatalytic properties.[13,23] Unfortunately, very little is known about the mechanism of the nucleation and growth of such heterostructures, and their synthesis is rather empirical. The general concept of growth of such materials is based on the nucleation of the second material on preformed seeds, and hence, the surface of seeds and its stability play the crucial role.

Chemical stability of the surface of transition-metal-based NCs is a very important issue for both catalytic and biomedical applications.[8,9] For example, cobalt-based NCs have higher saturation magnetization[24] as compared to iron oxides currently used as agents for MRI and hypothermia treatments; however, the potential leakage of cobalt ions is a serious concern that should be addressed. Cobalt ions can easily replace Zn and Mg active sites in coenzymes and lead to the generation of reactive oxygen species (ROS) that can provoke cancer.[25,26] On the other hand, the controlled release of metal ions from the surface of NCs capable of catalyzing the decomposition of H_2O_2 with the formation of ROS can be also beneficial. Thus, FePt NCs functionalized with cancer-targeting antibodies exhibited target-enhanced cytotoxicity to the tumor cells by release of iron ions.[9]

In addition, transition-metal-based nanostructures are of great interest for photochemical[27] and electrochemical water splitting.[28−30] These and other catalytic applications require control over chemical composition and electronic states of nanocrystals as well as their high stability.

Traditional physical methods of surface analysis such as X-ray photoelectron or X-ray absorption spectroscopy were proven to provide insights into composition and electronic states of the nanocrystals.[31] However, these analytic methods do not probe the surface layers exclusively and usually average the information over more than one monolayer. In addition, spectroscopic methods require certain sample preparation and data analysis that lead to relatively slow sample turnover and thus cannot be utilized for routine monitoring of the surface in time.

We report that the surface of metal nanocrystals can be probed by a chemiluminesence technique that allows us to monitor the presence of the transition-metal atoms at the NC surface and to detect their leaching into the solution. In this work, we also studied the ability of alloyed NCs to initiate the formation of ROS. Three different types of cobalt-based NCs were examined: (i) differently sized $CoPt_3$ NCs; (ii) Co NCs and (iii) $CoPt_3$/Au nanodumbbells.

Materials and Methods

Chemicals. Platinum acetylacetonate (Pt $(acac)_2$, Acros Organics, 98%), 1-adamantanecarboxylic acid (ACA, 99%, Aldrich), hexadecylamine (HDA, 90%, Aldrich), diphenyl ether (99%, Aldrich), cobalt carbonyl ($Co_2(CO)_8$, stabilized with 1−5% of hexane, Strem), 1,2-dichlorobenzene (anhydrous, 99%, Aldrich), trioctylphosphine oxide (TOPO, 99% Aldrich), oleic acid (OA, 90%, Aldrich), platinum(II) chloride ($PtCl_2$, 99.999%, Aldrich), didodecyldimethylammonium bromide (DDAB, 98%, Fluka), $NaBH_4$ (98.5%, Aldrich), toluene (99.5%, Aldrich), chloroform (99.9%, Aldrich), ethanol (anhydrous, ACS grade, Pharmaco-Aaper), 2-propanol (99.9%, Fisher Scientific), methanol (99.9% Riedel-de Haen), 1,2-dipalmitoyl-*sn*-glycero-3-phosphoethanolamine-*N*-[methoxy(polyethylene glycol)-2000] (PEG-PE) dissolved in chloroform (10 mg/mL solution, Avanti Polar Lipids, Inc.), 5,5-dimethyl-1-pyrroline *n*-oxide (DMPO, 97%, Sigma), $CoCl_2 \cdot 6H_2O$ (99.9%, Aldrich), H_2O_2 (30% Aldrich), and gold chloride ($AuCl_3$, 99.99%, Aldrich) were used as received without further purification.

Synthesis of $CoPt_3$ NCs. $CoPt_3$ NCs of different sizes were synthesized according to the modified protocol described in ref 32. Briefly, Pt $(acac)_2$ (33 mg) and ACA (0.25 g) were dissolved at 55 °C under nitrogen flow in a mixture of HDA (4 g) and diphenyl ether (2 mL). Then the solution was heated to 170 °C, and $Co_2(CO)_8$ dissolved in ∼1 mL of 1,2-dichlorobenzene was injected. The size of $CoPt_3$ NCs was controlled by the amount of $Co_2(CO)_8$. Thus, 0.106 g, 0.09 g, 0.068 g, 0.043 g, and 0.027 g of $Co_2(CO)_8$ were used to synthesize 4 nm, 4.8 nm, 6 nm, 8 nm, and 10.5 nm $CoPt_3$ NCs, respectively. No 1,2-hexadecanediol was used as compared with ref 32. After injection of cobalt carbonyl solution, the reaction mixture was kept at 170 °C for 1 h. NCs were annealed at ∼246 °C for 15−20 min, and then the reaction solution was cooled to 70 °C and 5 mL of chloroform was injected. The solution was then cooled to room temperature under ambient conditions.

Synthesis of $CoPt_3$−Au Dumbbell-like Heterodimers. Dumbbells of $CoPt_3$−Au were prepared via the modified procedure described in ref 33: $AuCl_3$ (8 mg), DDAB (54 mg), and HDA (74 mg) were dissolved in 4 mL of toluene by sonication for 15 min in the ultrasonic bath until a clear yellow solution was formed. A toluene solution of $CoPt_3$ containing 1.15 mg of 8 nm NCs was diluted to 3 mL and heated to 95 °C in a three-neck flask under nitrogen. $AuCl_3$ solution was then added dropwise (1 mL/h) via a syringe pump, and the solution was kept at 95 °C for an additional 2 h. The size of the Au portion of the nanodumbbells was found to be ∼11 nm.

Synthesis of Co NCs. Co NCs were synthesized according to the method proposed by Puntes et al.[34] TOPO (0.05 g) and OA (0.05 mL) were dissolved in 1,2-dichlorobenzene (7.5 mL) and heated to ∼182 °C under continuous stirring. Then, the solution containing $Co_2(CO)_8$ (0.27 g) and 1,2-dichlorobenzene (1.5 mL) was quickly injected, and the reaction mixture was kept at the reflux temperature for 5 min and then quickly cooled with water bath.

Synthesis of 4.5 nm Pt NCs. $PtCl_2$ (0.03 g) and DDAB (0.1 g) were dissolved in 10 mL of toluene by sonication for 30 min. After that, OA (0.2 mL) was added, and the reaction mixture was sonicated for an additional 5 min and quickly heated to 80 °C. A 40 μL portion of $NaBH_4$ solution in water (0.35 g/mL) was injected into the reaction mixture followed by immediate addition of HDA

(22) Wang, C.; Wei, Y. J.; Jiang, H. Y.; Sun, S. H. *Nano Lett.* **2009**, *9*, 4544–4547.
(23) Zhang, J.; Sasaki, K.; Sutter, E.; Adzic, R. R. *Science* **2007**, *315*, 220–222.
(24) Jeong, U.; Teng, X. W.; Wang, Y.; Yang, H.; Xia, Y. N. *Adv. Mater.* **2007**, *19*, 33–60.
(25) Hartwig, A. *4th Congress of Toxicology in Developing Countries*; IUPAC: Antalya, Turkey, 1999; pp 1007−1014.
(26) Hartwig, A.; Asmuss, M.; Ehleben, I.; Herzer, U.; Kostelac, D.; Pelzer, A.; Schwerdtle, T.; Burkle, A. *3rd International Meeting on the Molecular Mechanisms of Metal Toxicity and Carcinogenicity*; US Dept Health Human Sciences Public Health Science: Stintino, Italy, 2001; pp 797−799.
(27) Kay, A.; Cesar, I.; Gratzel, M. *J. Am. Chem. Soc.* **2006**, *128*, 15714–15721.
(28) Kanan, M. W.; Nocera, D. G. *Science* **2008**, *321*, 1072–1075.
(29) Surendranath, Y.; Dinca, M.; Nocera, D. G. *J. Am. Chem. Soc.* **2009**, *131*, 2615–2620.
(30) Risch, M.; Khare, V.; Zaharieva, I.; Gerencser, L.; Chernev, P.; Dau, H. *J. Am. Chem. Soc.* **2009**, *131*, 6936.
(31) Lee, W. R.; Kim, M. G.; Choi, J. R.; Park, J. I.; Ko, S. J.; Oh, S. J.; Cheon, J. *J. Am. Chem. Soc.* **2005**, *127*, 16090–16097.
(32) Shevchenko, E. V.; Talapin, D. V.; Schnablegger, H.; Kornowski, A.; Festin, O.; Svedlindh, P.; Haase, M.; Weller, H. *J. Am. Chem. Soc.* **2003**, *125*, 9090–9101.
(33) Pellegrino, T.; Fiore, A.; Carlino, E.; Giannini, C.; Cozzoli, P. D.; Ciccarella, G.; Respaud, M.; Palmirotta, L.; Cingolani, R.; Manna, L. *J. Am. Chem. Soc.* **2006**, *128*, 6690–6698.
(34) Puntes, V. F.; Zanchet, D.; Erdonmez, C. K.; Alivisatos, A. P. *J. Am. Chem. Soc.* **2002**, *124*, 12874–12880.

Table 1. PEG-PE Amounts Used for Water Transfer of Synthesized NCs

	NC′ diameter, nm	vol of PEG-PE solution per 1 mg of NCs (μL)
$CoPt_3$ NCs	4	124
	4.8	104
	8	62
	10.5	47
	6	83
Co NCs	9.5	153
Pt NCs	4.5	134
$CoPt_3$/Au dumbbells	8/11	76

(0.153 g). The solution was kept at 80 °C for 15 min. The inert atmosphere was not found to be important for synthesis of Pt NCs.

Postpreparative Procedures. As-synthesized particles were washed to remove the excess of stabilizers and byproducts by precipitation with alcohols (methanol, ethanol, 2-propanol) and centrifugation. The precipitates were redispersed in 2−3 mL of toluene or chloroform and filtered through a 0.2 μm PTFE filter.

Phase Transfer of NCs. NCs were transferred into water according to the protocol described in ref 35. The solutions of NCs were washed by multiple washing steps with alcohols. The first washing was performed using a mixture of methanol and ethanol. The second washing was performed with ethanol, and any other subsequent purification steps were performed with nonsolvents such as 2-propanol or ethanol/2-propanol mixture. The volume ratio of the NCs solution to the nonsolvent was usually 1:10. Final centrifugates were redissolved in 1 mL of chloroform, and PEGylated phospholipid (PEG-PE) dissolved in chloroform (10 mg/mL) solution was added. The volume of added PEG-PE solution was adjusted to obtain the ratio of PEG-PE molecules, and the number of atoms on the NCs' surface was approximately 1:5 (Table 1). In the case of $CoPt_3$/Au nanodumbbells, the amount of surface atoms was calculated by summation of surface atoms at the surface of $CoPt_3$ and Au counterparts. After addition of phospholipid, chloroform was evaporated completely under the nitrogen flow. The solid residue was heated to 80 °C, and 2 mL of hot deionized water was added. After cooling, the resulting aqueous solution was cleaned from the excess of phospholipid by centrifugation at 20000 rpm for 2 h. Final aqueous solutions were optically clear and stable for at least 2 weeks.

Dialysis. Aqueous solutions of NCs (1.5 mL) placed into the 0.5−3 mL Slide-A-Lyser dialysis cassette with molecular weight 3500 MWCO were dialyzed versus 300 mL of DI water under stirring. After the dialysis was stopped, the solution was evaporated slowly at 50 °C until its volume became 1.5 mL (equal to the volume of the NCs solution inside the cassette). Both dialysis water and NCs solution taken out from the cassette were tested in the CL experiments.

The X-ray diffraction data (XRD) were collected using a Bruker D8 Discover diffractometer (Cu Kα radiation, 0.1 mm detector slit). Samples for transmission electron microscopy (TEM) were prepared by droping and drying of 1−2 μL of toluene solution of NCs on a carbon-coated copper grid (Ted Pella).

Fourier transform infrared (FTIR) measurements were conducted using a Bruker (Billerica, MA) Vertex 70 spectrometer. Films containing of ~100 μg of NCs were directly placed on top of the sample stage of the switchable attenuated total reflection (ATR) device. Thermogravimetric analysis (TGA) was performed using Mettler Toledo 851 apparatus. The initial amount of the sample for TGA measurements was not less than 3 mg; the samples were loaded into a light aluminum crucible by dropping and drying the concentrated NC solution. All measurements were done under continuous nitrogen flow. The ξ-potential measurements of NCs were performed on ZetaSizer (Mavern Instruments) operating at 633 nm laser wavelength, in the voltage range of 0.5−40 V. ξ-Potentials of NCs were measured at 30 and 2 V in chloroform and in water, respectively. The distance between electrodes was 0.4 cm. The Smoluchowski model was chosen for ξ-potential calculations. X-ray photoelectron spectroscopy (XPS) measurements were performed with synchrotron radiation at the beamline BW3 at HASYLAB/DESY in Hamburg, Germany. Samples were prepared by drop-casting $CoPt_3$ NCs from colloidal solution on cleaned Au substrates. XP spectra were recorded with an Omicron EA 125 hemispherical electron analyzer. Peak fitting was done with Voigt line shapes and a combined polynomial and Shirley-type background function. The binding energy scale was referenced to the Au $4f_{7/2}$ level of the substrates that was set to 84.0 eV binding energy according to ref 36. Electron paramagnetic resonance (EPR) spectra were obtained using a Bruker Elexys E580 spectrometer. All experiments were conducted at room temperature. DMPO spin trap was used, and all solutions were prepared under aerobic conditions. Stock solutions for the EPR reaction mixture preparation were 1.2 M aqueous solution of DMPO, 0.4 mM solution of $CoCl_2$ 0.88 M solution of H_2O_2, aqueous solution of 6 nm $CoPt_3$ NCs with surface Co atoms concentration of 2.32 mM ($[Co_{surf}]$) calculated assuming that the amount of Co atoms on the surface corresponds to general alloy NC stoichiometry (75% Pt atoms per 25% Co atoms) and aqueous solution of Pt NCs with 9.64×10^{11} particles in 1 μL ($[Pt_{surf}] = 1.78$ mM). For EPR measurements, 10 μL of DMPO stock solution was mixed with 10 μL of stock solutions of other reagents in order to scavenge possible ROS and finally diluted with DI water to a volume of 80 μL. Sample solutions were placed in a d ~1 mm quartz tube, and EPR spectra were measured immediately after sample preparation (9.4 GHz, power 33 mW, modulation amplitude 1 G). All sample preparations and measurements except otherwise stated were conducted under aerobic atmosphere. Magnetic properties were studied using SQUID magnetometry (MPMS XL, Quantum Design). The spectra of chemiluminescence (CL) were measured with a Perkin-Elmer LS 55 spectrometer. CL signals were collected by a custom-made setup consisting of a Si-based light flux detector (THOR Laboratories, DET 100A) coupled with a digital storage oscilloscope (Tektronix, TSD 2014B). Samples were placed in disposable 1 cm plastic cuvettes. Cuvettes were positioned 2 cm from the detector. In a typical experiment, 1 mL of luminol solution (1.13 mM) in carbonate buffer (pH = 9) was mixed with NCs solution or/and cobalt chloride solution. The total volume of solutions containing NCs or Co^{2+} ions was within the range of 0.5−600 μL. DI water was used to dilute the final volume of the sample up to 1.7 mL to simplify the normalization. After that, 0.3 mL of H_2O_2 solution (44 mM) were quickly injected into luminol solution under vigorous stirring. Calibration was performed with blank solutions of $CoCl_2$ with seven different concentrations: 2, 4, 20, 40, 200, 400, and 1600 μM. The volume of the standard solutions taken for the CL reaction was 250 μL. Thus, final Co^{2+} concentrations were 0.25, 0.5, 2.5, 5, 25, 50, and 200 μM, respectively. The CL signal was registered with an oscilloscope. Quantitative information of the CL intensity was obtained by integration of CL signal over time (Figure S1, Supporting Information).

Results and Discussion

$CoPt_3$ NCs of five different sizes were synthesized in high-boiling solvent (Figure 1). All particles have a chemically disordered face-centered cubic (fcc) phase as previously reported.[13,32] $CoPt_3$ NCs were transferred into water using the phospholipids (see Phase Transfer of NCs in the Materials and Methods). We have found that multistep washing of NCs is critical for the phase transfer. According to the TGA data, there is ~45 wt % of organic molecules in the sample of 8 nm $CoPt_3$ NCs after basic purification of NCs from the excess of precursors

(35) Dubertret, B. *M/S: Medecine Sci.* **2003**, *19*, 532–534.

(36) Powell, C. J. *Appl. Surf. Sci.* **1995**, *89*, 141–149.

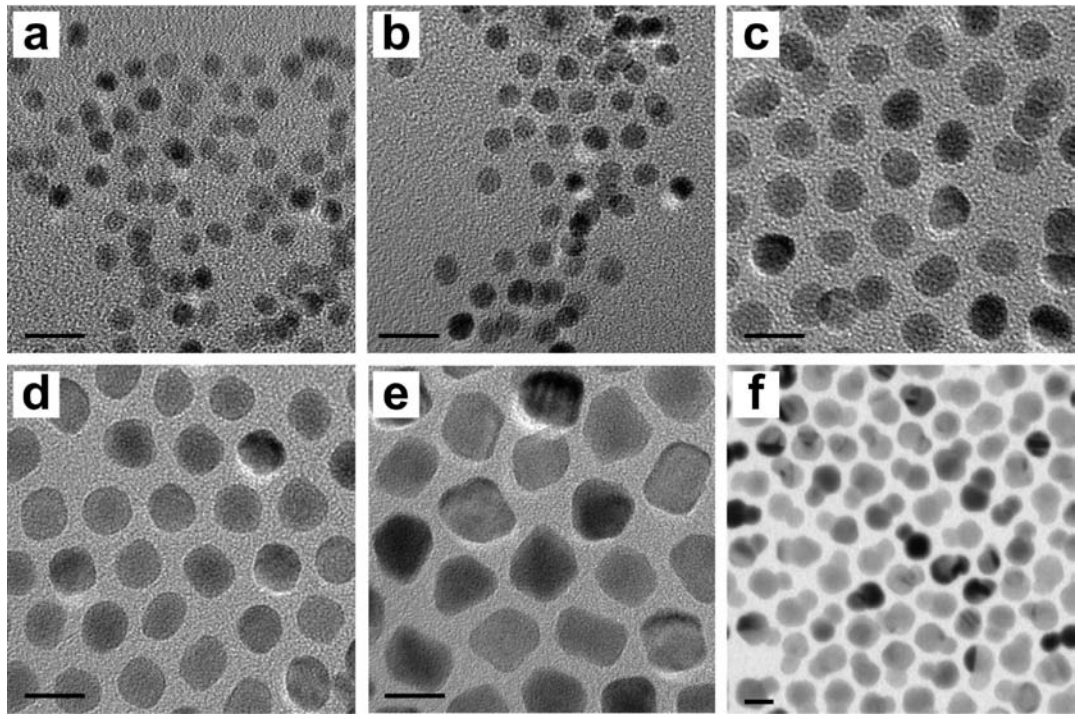

Figure 1. TEM overview images of 4.0, 4.8, 6.0, 8.0, and 10.5 nm $CoPt_3$ NCs and $CoPt_3$/Au (8 nm/11 nm), respectively (a−f). Scale bars are 10 nm.

and byproduct (Figure S2, Supporting Information). The solutions of such samples in toluene or chloroform were stable against aggregation and oxidation for months; however, NCs could not be transferred into water. The subsequent purification procedures reduced the concentration of the organic component down to ∼5−6% that was optimal for phase transfer from chloroform into water. To calculate the weight of ligand monolayer on the NC surface, we assumed a 1:3 ratio of ACA to HDA assuming a 1:3 ratio of Co to Pt. The footprint of HDA is 18.6−20 Å,[2,37,38] and the cross-section of ACA is calculated to be 23−28 $Å^2$ on the basis of the effective diameter of the molecule reported in ref 39. According to the calculations, 5−6 wt % of organic molecules cannot provide the full passivation of the surface of 8 nm $CoPt_3$ NCs that obviously can facilitate the phase transfer. FTIR measurements (Figure S3, Supporting Information) indicate the higher concentration of chlorine containing organics in the properly washed samples. This signal can originate from the absorbed molecules of chloroform that was used as a solvent, confirming the lack of HDA and ACA molecules at the surface of NCs.

It is well-known that cations of transition metals (e.g., Co^{2+}, Fe^{2+}, Ni^{2+}, etc.) can induce Fenton-type chemical reactions and lead to the formation of free radicals $O_2^{\bullet-}$, $OH^{\bullet}$, and $OOH^{\bullet}$ that are called reactive oxygen species.[40,41] The generation of ROS is an important stage in oxidation of luminol (Scheme S1).[42−44] The oxidation of luminol is accompanied by intense emission of a blue light in the process known as chemiluminesence

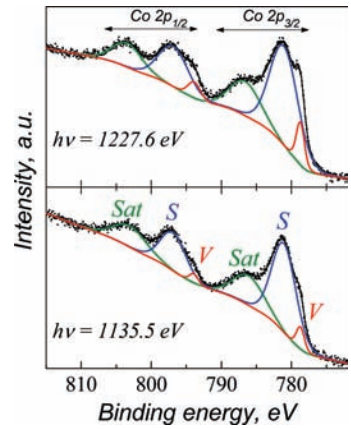

Figure 2. XPS spectra of 8 nm $CoPt_3$ NCs in the energy regions of the Co 2p bands at two different photon energies. Experimental data (dotted curves) are plotted together with a deconvolution into contributing peaks (solid curves).

(CL).[45−50] This highly sensitive reaction[51,52] is routinely used in forensic medicine to detect trace amounts of blood since blood

(37) Plaut, D. J.; Lund, K. M.; Ward, M. D. *Chem. Commun.* **2000**, 769–770.
(38) Espina, A.; Garcia, J. R.; Guil, J. M.; Jaimez, E.; Parra, J. B.; Rodriguez, J. *J. Phys. Chem. B* **1998**, *102*, 1713–1716.
(39) Valyon, J.; Engelhardt, J. *React. Kinet. Catal. Lett.* **1998**, *63*, 27–32.
(40) Gutteridge, J. M. C. *Free Radical Res. Commun.* **1993**, *19*, 141–158.
(41) Konovalova, T. A.; Lawrence, J.; Kispert, L. D. *J. Photochem. Photobiol. A: Chem.* **2004**, *162*, 1–8.
(42) Baj, S.; Krawczyk, T. *J. Photochem. Photobiol. A: Chem.* **2006**, *183*, 111–120.
(43) Mercnyi, G.; Lind, J.; Eriksen, T. E. *J. Phys. Chem.* **1984**, *88*, 2320–2323.
(44) Rose, A. L.; Waite, T. D. *Anal. Chem.* **2001**, *73*, 5909–5920.
(45) Lind, J.; MerBnyi, G.; Eriksen, T. E. *J. Am. Chem. Soc.* **1983**, *105*, 7655–7661.
(46) Burdo, T. G.; Seitz, W. R. *Anal. Chem.* **1975**, *47*, 1639–1643.
(47) Kitajima, N.; Fukuzumi, S.; Ono, Y. *J. Phys. Chem.* **1978**, *82*, 1505–1509.
(48) Lin, J. M.; Shan, X. Q.; Hanaoka, S.; Yamada, M. *Anal. Chem.* **2001**, *73*, 5043–5051.
(49) Ren, J. C.; Huang, X. Y. *Anal. Chem.* **2001**, *73*, 2663–2668.
(50) Du, J. X.; Li, J. J.; Yang, L. L.; Lu, J. R. *Anal. Chim. Acta* **2003**, *481*, 239–244.
(51) Rongen, H. A. H.; Hoetelmans, R. M. W.; Bult, A.; Vanbennekom, W. P. *J. Pharm. Biomed. Anal.* **1994**, *12*, 433–462.
(52) Dodeigne, C.; Thunus, L.; Lejeune, R. *Talanta* **2000**, *51*, 415–439.

contains iron-based oxygen-transport metalloprotein (hemoglobin) that can promote the generation of ROS.[53,54] Other transition-metal ions in the oxidation state +2 (e.g., Co^{2+}, see the reactions 1−5 below) can also lead to the formation of ROS that further oxidize the luminol into aminophthalate. Note that during this reaction M^{2+} ions converts irreversibly into M^{3+}, and hence, M^{2+} ions are not recycled as a true catalyst. The intensity of CL is proportional to the concentration of M^{2+} ions at their high dilutions that is used to determine quantitatively the low (nM) concentrations of these ions.

$$Co(II) + O_2 \rightarrow Co(III) + O_2^{\bullet -} \quad (1)$$

$$Co(II) + O_2^{\bullet -} \xrightarrow{2H^+} Co(III) + H_2O_2 \quad (2)$$

$$Co(II) + H_2O_2 \rightarrow Co(III) + OH^{\bullet} + OH^- \quad (3)$$

$$Co(II) + OH^{\bullet} \rightarrow Co(III) + OH^- \quad (4)$$

$$Co(III) + H_2O_2 \rightarrow Co(II) + OOH^{\bullet} + H^+ \quad (5)$$

We employed the chemiluminescence technique based on the oxidation of luminol to analyze the surface of NCs containing atoms of transition metals. $CoPt_3$-based NCs (individual $CoPt_3$ NCs and $CoPt_3$/Au dumbbells) were chosen as the model system (i) because these NCs can be synthesized in a wide size range with narrow size distribution (Figure 1) and (ii) because of the relatively long decay times of the CL promoted by cobalt ions (Figure S1).

XPS analysis of $CoPt_3$ NCs revealed the presence of different types of Co species in the NCs (Figure 2). The doublet labeled "V" in Figure 2 has a binding energy of 778.8 eV for the Co $2p_{3/2}$ level and a spin−orbit splitting of 15.2 eV. These values are in good agreement with reference data for metallic Co.[55] We assigned this doublet to Co atoms in the volume of the bimetallic particles. The second doublet, labeled "S", was observed at ~781 eV ($2p_{3/2}$) with a larger spin−orbit splitting of ~15.8 eV. These values are typical for cobalt in the oxidation state Co^{2+}, as it was previously observed in spectra of CoO[56] The third doublet, labeled "Sat" can be identified as a shakeup satellite feature.[56] We assign the component "S" to Co^{2+} surface sites that are coordinated by the ACA ligands.

It was indeed assumed previously that ACA molecules bind preferably to the Co surface sites and Pt surface atoms are coordinated by HDA.[15,57,58] Coordinated oxidized cobalt surface sites may contribute to the component "S" as well. Note also that this component is very broad, suggesting inhomogeneous broadening due to the presence of Co^{2+} species in slightly different chemical environments that cannot be further resolved, e.g., oxidized cobalt surface sites and surface sites capped with the ACA ligands.

(53) Zhou, S. L.; Wang, J. H.; Huang, W. H.; Lu, X.; Cheng, H. K. *J. Chromatogr. B: Anal. Technol. Biomed. Life Sci.* **2007**, *850*, 343–347.
(54) Zhi, Q.; Xie, C.; Huang, X. Y.; Ren, J. C. *Anal. Chim. Acta* **2007**, *583*, 217–222.
(55) Mandale, A.; B, B. S.; Date, S. K J. *J. Electron Spectrosc. Relat. Phenom.* **1984**, *33*, 61–72.
(56) Chuang, T. J. B. C. R.; Rice, D. W. *Surf. Sci.* **1976**, *59*, 413–429.
(57) Samia, A. C. S.; Schlueter, J. A.; Jiang, J. S.; Bader, S. D.; Qin, C. J.; Lin, X. M. *Chem. Mater.* **2006**, *18*, 5203–5212.
(58) Bagaria, H. G.; Ada, E. T.; Shamsuzzoha, M.; Nikles, D. E.; Johnson, D. T. *Langmuir* **2006**, *22*, 7732–7737.

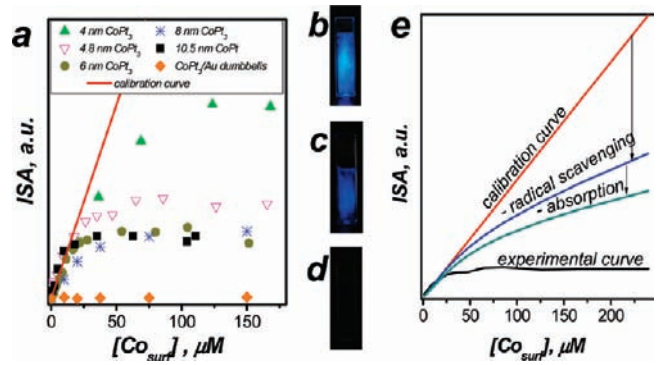

Figure 3. (a) Dependence of the integrated surface area (ISA) on the concentration of cobalt atoms at the surface([Co_{surf}]) of differently sized $CoPt_3$ NCs and the calibration plot obtained with solutions of $CoCl_2$ of different concentrations; (b−d) optical images of chemiluminesence made at the decay time of 0.2 s in of the solutions of 53 μM $CoCl_2$, 4.8 nm $CoPt_3$ NCs with [Co_{surf}] = 65 μM and $CoPt_3$/Au dumbbells, respectively; (e) summary of different contributing factors (scavenging of radicals at the surface of 4.8 nm $CoPt_3$ NCs and losses of signal due to absorption of emitted light by NCs) that describe the lower CL signal in case of NCs as compared with calibration $CoCl_2$ solution.

Since Co^{2+} ions can be oxidized by oxygen and peroxide in alkaline solutions,[40,41] we expected that cobalt atoms at the surface of NCs can also promote the formation of ROS and induce the oxidation of luminol. Indeed, Figure 3 provides the visualization of the CL promoted by cobalt ions in solution and by the surface of $CoPt_3$ NCs.

The spectrum of CL exhibits a maximum at 420 nm (Figure S1a, Supporting Information). The integrated signal area (ISA) of the CL intensity was chosen as a parameter minimizing the effect of fluctuations in mixing of injected peroxide solution (Figure S1b, Supporting Information). The calibration curve of ISA versus [Co^{2+}] shows linear dependence in the concentration range of 0−200 μM (Figure S4, Supporting Information). Further increase of [Co^{2+}] results in the formation of $Co(OH)_2$ that precipitates from the solution leading to the drop in CL signal (Figure S4, Supporting Information).

We measured the ISA of CL as a function of concentration of cobalt atoms [Co_{surf}] at the surface of $CoPt_3$ NCs of different sizes. We used the following assumptions: (i) the ratio of Co to Pt atoms at the surface of NCs is equal 1:3 (the elemental analysis is in a good agreement with $CoPt_3$ stoichiometry (Table S1, Supporting Information), and (ii) we assumed that all surface atoms of cobalt are chemically active. The weighting of the dried samples and subtracting the amount of organic molecules determined by TGA allows us to calculate the number of individual NCs in studied samples based on their sizes determined from TEM. Figure 3a shows the plots of ISA of CL versus the concentration of surface atoms of cobalt [Co_{surf}] for five different sizes of $CoPt_3$ NCs. The dependence of ISA on the [Co_{surf}] is linear only at very high dilutions of NCs. The deviation of the slope of linear part of the curves from the slope of the calibration curve can originate from faceting of NCs that can provide higher or lower concentration of surface atoms of cobalt. In addition, not all surface atoms of cobalt can participate in the generation of ROS. Further increase of NC concentrations leads to the saturation of the ISA curves in all five cases of NC sizes. In order to understand this observation, we studied the role of the factors discussed below. First, we examined the effect of PEG-PE used to transfer NCs into water. However, the addition of PEG-PE to the Co^{2+} solution in the same concentration of lipids per cobalt atom as in the case of $CoPt_3$ samples

did not affect the intensity of the CL signal. To figure out the contribution of light absorption by $CoPt_3$ NCs into losses of CL we examined the ISA of Co^{2+} solution under different concentrations of "inactive" $CoPt_3$ NCs (during the oxidation of luminol cobalt(II) is irreversibly converted into Co(III) and thus, the addition of extra portions of H_2O_2 and luminol suppresses the activity of $CoPt_3$ NCs in generation of ROS (see the Supporting Information for details)). The absorption of light by $CoPt_3$ NCs can lead to the drop in the intensity of CL (Figure S5, Supporting Information); however, it cannot explain all losses of ISA, and other factors have to be taken into consideration.

It is known that platinum can catalyze the H_2O_2 disproportionation reaction.[59]

$$2H_2O_2 \xrightarrow{Pt} 2H_2O + O_2 \qquad (6)$$

The proposed mechanism of this reaction is based on the formation of $Pt-(OH_{ads})$ and $Pt-(OOH_{ads})$ complexes adsorbed at the surface of NCs.[60] In addition to that, the platinum surface is known to be a good scavenger for the ROS.[61] We decided to examine the possibility of radical scavenging by Pt and $CoPt_3$ NCs. For that, we added different amounts of $CoPt_3$ and Pt NCs to the solutions of cobalt(II) chloride. We normalized the concentration of both $CoPt_3$ and Pt NCs to the concentration of surface platinum assuming the spherical shape of NCs. Addition of both $CoPt_3$ and Pt NCs to the solutions of $CoCl_2$ led to a significant decrease of CL (Figure S6, Supporting Information). Using experimental data presented in Figures S5 and S6 (Supporting Information), we can estimate the ISA/$[Co_{surf}]$ dependences after subtraction of absorption and radical scavenging losses form calibration curve. As we can see, light absorption and scavenging of radicals at the surface of NCs explains ~70% of the deviation of the experimental results obtained on $CoPt_3$ NCs from the calibration curve (Figure 3e). In addition, it was shown that noble metal NCs are able to accumulate negative charge during their synthesis.[62] Thus, we have to consider the possibility of the chemisorption of the metal cations from the solution at the surface of NCs due to Coulomb attraction. The measurements of the ξ-potential on $CoPt_3$ and Pt NCs indicate that both types of NCs can adsorb Co^{2+} ions (Figure S6, insert, Supporting Information) decreasing the effective concentration of Co^{2+} ions in the solution. Based on the same trend in change of ξ-potential, we can assume that $CoPt_3$ and Pt NCs adsorb similar amount of cobalt ions. This adsorption may result in the decrease of the amount of active Pt sites on the NCs' surface, potentially causing underestimation of the scavenging effect of surface Pt atoms. In addition to that, we cannot exclude the effect of passivation of Pt surface by PEG-PE that can also depends on size and faceting of NCs. In our experiment, we used only 4.5 nm Pt NCs; the size of those is close to the size of 4.8 nm $CoPt_3$ NCs.

As shown in Figure S6 (Supporting Information), higher dilutions of $CoPt_3$ NCs demonstrate CL quenching almost two times stronger as compared to Pt NCs, which is rather

Scheme 1. Depiction of the DMPO Adducts with $^{\bullet}OH$ and $O_2^{\bullet-}$/$HOO^{\bullet}$ Radicals[65]

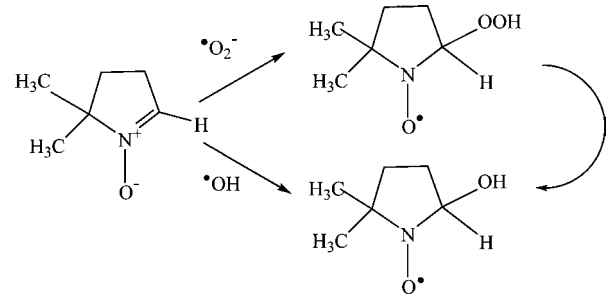

counterintuitive. We assume that platinum at the surface of $CoPt_3$ NCs can scavenge the ROS more efficiently than Pt NCs. Previously, it was shown experimentally and explained theoretically that small Pt clusters and *ad*-islands were better catalysts than Pt NCs.[63,64] In addition, the better performance of Pt-based alloys as compared with pure platinum was found to occur due to the change of electronic structure of platinum.[11] All three scenarios can affect the calculation accuracy in the case of modeling $CoPt_3$ NCs by addition of Pt NCs to Co^{2+} solution.

To prove the ROS scavenging ability of Pt and $CoPt_3$ NCs, we carried out the room-temperature EPR experiments. The DMPO was used as a spin-trap agent (Scheme 1). The concentrations of the reaction species used in EPR experiments were increased as compared to those in the CL experiments due to the lower sensitivity of the spin-trapping method. Blank experiments with H_2O_2 and DMPO do not show any adduct radical product (Figure 4). Addition of Pt NCs to H_2O_2 and DMPO solution does not result in radical production as well. However, the formation of gaseous products can be observed even by the naked eye. The catalytic decomposition of H_2O_2 on platinum involves dissociation of peroxide on the Pt surface with formation of strongly adsorbed $OH^{\bullet}$ radicals that further convert into oxygen and water.[60]

In the case when Co^{2+} and H_2O_2 were mixed with DMPO under anaerobic conditions, the EPR revealed a four-line spectrum with $g = 2.0057$ and hyperfine splitting $a_N = 14.9$ G (Figure 4). According to the literature, the spectrum can be attributed to the DMPO−OH adduct.[65] The same measurements performed in the presence of air revealed superposition of a new signal with $g = 2.0058$ and $a_N = 13.9$ G that corresponds to the DMPO-OOH adduct[65,66] (Figure 4). In Figure 4, the lines corresponding to DMPO-OH radicals are labeled by circles, while ones corresponding to DMPO-OOH radical adducts are labeled with stars. The DMPO-OOH radical adduct is not stable, and its transformation to DMPO-OH, according to Scheme 1, was completed in 20 min (Figure 4).

The formation of $^{\bullet}OH$ and $^{\bullet}OOH/O_2^{\bullet-}$ radicals can lead to the oxidation of luminol (Scheme S1, Supporting Information). The addition of Pt NCs to the Co^{2+}/H_2O_2/DMPO mixture results in much lower peak intensities (Figure 4), confirming efficient scavenging of the radicals by Pt NCs. The formation

(59) Qin, L. D.; Banholzer, M. J.; Xu, X. Y.; Huang, L.; Mirkin, C. A. *J. Am. Chem. Soc.* **2007**, *129*, 14870.
(60) Mededovic, S.; Locke, B. R. *Appl. Catal. B* **2006**, *67*, 149–159.
(61) Hamasaki, T.; Kashiwagi, T.; Imada, T.; Nakamichi, N.; Aramaki, S.; Toh, K.; Morisawa, S.; Shimakoshi, H.; Hisaeda, Y.; Shirahata, S. *Langmuir* **2008**, *24*, 7354–7364.
(62) Henglein, A. *J. Phys. Chem.* **1993**, *97*, 5457–5471.
(63) Vajda, S.; Pellin, M. J.; Greeley, J. P.; Marshall, C. L.; Curtiss, L. A.; Ballentine, G. A.; Elam, J. W.; Catillon-Mucherie, S.; Redfern, P. C.; Mehmood, F.; Zapol, P. *Nat. Mater.* **2009**, *8*, 213–216.
(64) Strmcnik, D. S.; Tripkovic, D. V.; van der Vliet, D.; Chang, K. C.; Komanicky, V.; You, H.; Karapetrov, G.; Greeley, J.; Stamenkovic, V. R.; Markovic, N. M. *J. Am. Chem. Soc.* **2008**, *130*, 15332–15339.
(65) Mojovic, M.; Spasojevic, I.; Vuletic, M.; Vucinic, Z.; Bacic, G. *J. Serb.Chem. Soc.* **2005**, *70*, 177–186.
(66) Kadiiska, M. B.; Maples, K. R.; Mason, R. P. *Arch. Biochem. Biophys.* **1989**, *275*, 98–111.

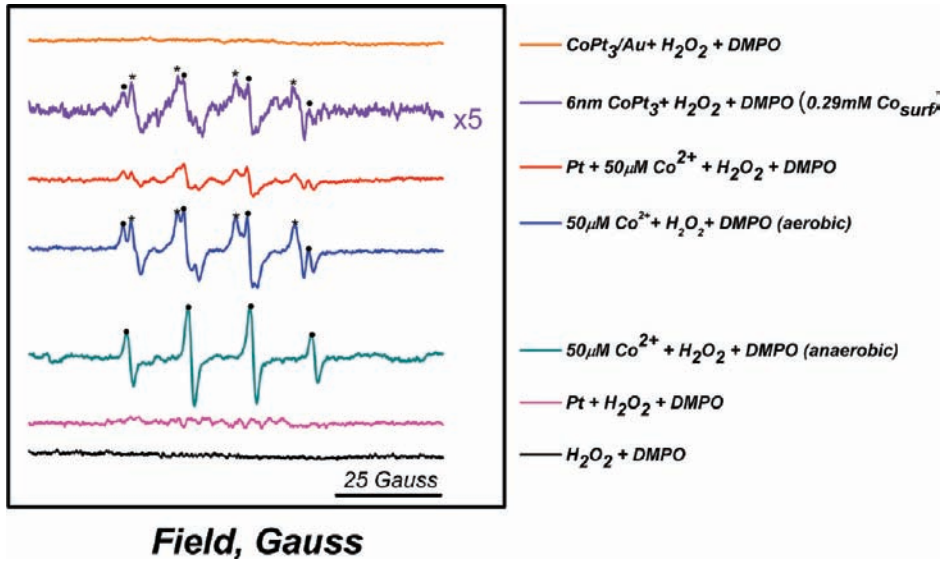

Figure 4. EPR spectra of DMPO adduct radicals formed in the presence of •OH and •OOH radicals. DMPO-OH and DMPO-OOH peaks are depicted by circles and stars, respectively. In all experiments, the concentrations of H_2O_2 and DMPO were 0.11 and 0.15 M, respectively.

of small amounts of DMPO-OH and DMPO-OOH was observed even though the sample was prepared and kept under nitrogen atmosphere during the measurements. This observation indicates the generation of oxygen catalyzed by Pt (eq 6) that can be further converted into •OH and $O_2^{\bullet-}$ in the presence of Co^{2+}. Addition of $CoPt_3$ NCs to the Co^{2+}/H_2O_2/DMPO mixture demonstrates a substantial decrease in the radical production efficiency comparative to Co^{2+} similar to the case of Co^{2+} ions and Pt NCs mixture.

For comparison purposes, we also performed experiments with pure 9.5 ± 1.5 nm Co NCs (Figure S7, Supporting Information). Co NCs were also found to promote the oxidation of luminol. However, addition of cobalt NCs into an alkaline solution of luminol was accompanied by a color change from black to greenish, indicating possible dissolution of cobalt NCs. Indeed, ISA-[Co] plots calculated with the assumption that there was no nanocrystal dissolutions are far above the calibration plot, confirming the leaching of cobalt ions from the nanocrystals (Figure S7, Supporting Information). The ease of dissolution of pure Co NCs prompted the idea that cobalt atoms can also leave the surface of $CoPt_3$ NCs, leaving a Pt-enriched surface layer that could be very beneficial for further catalytic applications.[67,68] In addition to that, washing out the interfacial atoms of transition metals can lower the toxicity of transition-metal-based magnetic NCs and potentially allow their biomedical applications (e.g., magnetic drug delivery, MRI agents) without the risk of deleterious side effects.

We found that continuous dialysis of $CoPt_3$ NCs in deionized water results in the leaching of cobalt atoms from the surface of NCs (Figure 5). We monitored the rate of dissolution of the surface cobalt using the chemiluminescence technique. Both dialysis water and solution of NCs were measured at different intervals of dialysis. The dialysis water was concentrated up to 1.5 mL. Note that the summation of ISA signals of dialysis water and solution of NCs at later stages of dialysis gives the

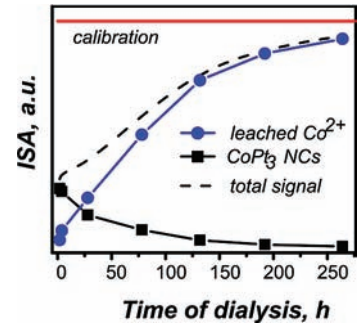

Figure 5. Kinetic of dialysis for 6 nm $CoPt_3$ NCs: the signal measured from Co^{2+} leached into water (blue line with circles); from $CoPt_3$ NCs (black line with squares) and summation of signals measured from leached Co^{2+} and from $CoPt_3$ NCs in dialysis cassette (black dashed line). Calibration curve (red line) corresponds to the $[Co_{surf}] = 70\ \mu M$ calculated for 6 nm $CoPt_3$ NCs assuming their spherical shape and 25% and 75% of Co and Pt NCs, respectively.

higher numbers approaching the CL signal for $[Co_{surf}]$ calculated for 6 nm large $CoPt_3$ NCs. After ~11 days of dialysis, the concentration of Co^{2+} in dialysis water almost reaches the concentration corresponding to the maximum concentration of cobalt atoms at the surface of 6 nm $CoPt_3$ NCs assuming the spherical shape of NCs and 1:3 stoichiometry.

This observation allows us to assume that cobalt atoms leach only from the surface of $CoPt_3$ NCs. The magnetic measurements performed on 4.8 nm $CoPt_3$ NCs before and after 11 days of dialysis show that these nanocrystals do not exhibit significant differences (Figure 6). There is about a 14% decrease in the coercivity and a minor decrease in the saturation magnetization. These changes can be attributed to the removal of the cobalt atoms from the surface of NCs. Since the impact of the canted spins of surface atoms into the total magnetization of the particle is lower than the impact of "bulk" spins,[69,70] the small losses in saturation magnetization are in good agreement with the removal of surface atoms, even though the concentration of total number of cobalt atoms at the surface of $CoPt_3$ NCs is relatively

(67) Stamenkovic, V. R.; Fowler, B.; Mun, B. S.; Wang, G. F.; Ross, P. N.; Lucas, C. A.; Markovic, N. M. *Science* **2007**, *315*, 493–497.
(68) Stamenkovic, V.; Mun, B. S.; Mayrhofer, K. J. J.; Ross, P. N.; Markovic, N. M.; Rossmeisl, J.; Greeley, J.; Norskov, J. K. *Angew. Chem., Int. Ed. Engl.* **2006**, *45*, 2897–2901.
(69) Kachkachi, H.; Ezzir, A.; Nogues, M.; Tronc, E. *Eur. Phys. J. B* **2000**, *14*, 681–689.

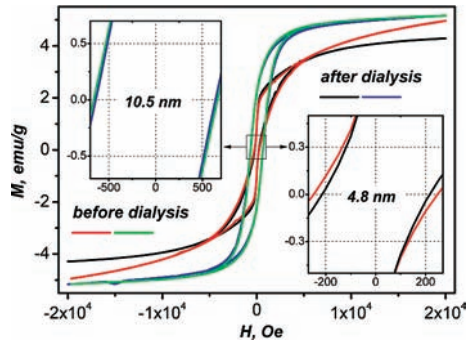

Figure 6. Magnetization curves of 4.8 and 10.5 nm $CoPt_3$ NCs at 5 K before and after dialysis. The duration of dialysis was 11 days.

high (~31%). The dialysis of larger 10.5 nm NCs that have ~14% Co atoms on their surface did not affect their magnetic properties. There were no measurable changes in coercivity and saturation magnetization (Figure 6). These results can be explained both by higher chemical stability of larger NCs due to their lower chemical potential[71] and by lower concentration of cobalt atoms at the surface of NCs. The FC and ZFC temperature dependencies of the magnetization of the sample before and after dialysis do not exhibit significant difference as well (Figure S8, Supporting Information). These data allows us to assume that in the case of as-transferred into water $CoPt_3$ nanoparticles CL comes mainly from the surface of NCs since the leaching of cobalt atoms is a slow process whereas CL decays very fast (days vs seconds).

The third tested system was $CoPt_3$/Au dumbbell-like NCs (Figure 1f). The gold containing NCs were proven to be very promising agents for diagnostics[8] and therapeutic treatment purposes.[72,73] The 11 ± 1 nm gold counterparts were grown on the presynthesized 8 nm $CoPt_3$ NCs. The composition of the $CoPt_3$/Au nanodumbbells was examined by EDX analysis, and the atomic ratio of Co/Pt/Au was about 1/2.95/9.9. No detectable CL signal was observed when $CoPt_3$/Au nanodumbbells were added to the solution of luminol instead of $CoPt_3$ NCs (Figure 3a,d). EPR data showed that the formation of hydroxyl and/or superoxide radicals does not occur in the case of dumbbell NCs (Figure 4). There are several factors that can lead to that observation. First, it can be associated with the synergetic effect of gold and platinum surfaces that act as the ROS scavengers. Addition of 15 nm Au NCs to the solution of $CoPt_3$ NCs results in the significant quenching of the CL signal (Figure S9, Supporting Information). For instance, 175 μM of Au NCs leads to ~43% decrease in CL signal of $CoPt_3$ NCs that is about two times more than CL losses induced by the same concentration of Pt NCs (~19%). In the case of the $CoCl_2$ solution, the same concentration of Au NCs causes the decrease in the intensity of CL signal of ~23% that is comparable to the CL losses caused by Pt NCs (~19%). Note, in this case the surface of Au NCs can absorb ions of cobalt that can potentially lower the concentration of cobalt ions in the solution. We assume that the adsorption of Co^{2+} takes place because there is a significant shift (~25 nm) of the plasmon resonance peaks to the red[62] (Figure S8, Supporting Information), and no aggregation of Au NCs took place as it was confirmed by light scattering experiments. We suggest that the adsorbed Co^{2+} ions can still participate in the generation of ROS since even cobalt atoms located at the surface of NCs can promote their formation as it was shown above. Two times stronger quenching of the CL in the case of $CoPt_3$ NCs by Au NCs as compared to the solution of Co^{2+} ions can originate from the difference in the kinetics of ROS generation by free ions in the solution and atoms at the surface of $CoPt_3$ NCs and by higher probability of the collision of ROS generated at the surface of $CoPt_3$ NCs and Au NCs as compared to the case of the solution of ions. The second reason of zero activity of $CoPt_3$/Au nanodumbbells in the promotion of ROS formation can be that there are no cobalt atoms in the appropriate form at the surface of $CoPt_3$ part in heterodimers. We can assume that the mechanism of the formation of $CoPt_3$/Au nanodumbbells can involve either oxidation of surface cobalt atoms into Co(III) or their leaching from the surface of $CoPt_3$ during nucleation and growth of Au counterpart. The mechanism of the $CoPt_3$/Au nanodumbbells formation is currently under investigation.

The results obtained for $CoPt_3$/Au nanodumbbells indicate that the toxicity of NCs associated with their ability to promote the formation of ROS can be significantly lowered by the proper design of NCs. Thus functionalization of transition metal based magnetic NCs with material (for instance gold) that can both scavenge the radicals and render them ease of further biofunctionalization can be a promising way toward high performance and safe agents for magnetic hyperthermia and MRI.

Conclusions

We have proposed a simple chemiluminescence-based method of investigation of surface properties of Co-containing nanocrystals. The CL method allows efficient monitoring over time of the stability of transition-metal NCs against oxidation and dissolution. This method reveals high sensitivity to only surface atoms. Using a combination of the chemiluminsence method and spin-trap EPR techniques, we studied the generation of ROS at the surface of different types of NCs. In fact, the findings from both techniques correlate very well. We have shown that differently sized $CoPt_3$ NCs can promote the formation of ROS and as a result can lead to the oxidation of luminol accompanied by emission of light. On the other hand, $CoPt_3$ NCs can serve as even better scavengers for ROS than Pt NCs. We observed by CL method that cobalt atoms slowly leach from the surface of $CoPt_3$ NCs even under very mild conditions; however, the concentration of the leached cobalt atoms does not exceed the maximal concentration of cobalt calculated assuming the spherical shape and 1:3 stoichiometry indicating that only surface atoms go into solution. Since the formation of layers of Pt at the surface of alloyed NCs (Pt skin) results in the superior catalytic performance of such materials, the leaching of cobalt atoms from the surface can be potentially beneficial to prepare highly efficient catalysts. Since only the dissolution of the atoms of transition metals from the surface of alloy NCs occurs and further leaching of their atoms has not been found, alloy NCs based on transition metals other than iron can be considered as alternative for iron-based nanostructures for biomedical applications.

We believe that our method can be also utilized to monitor the stability of the shell grown around the transition metal based nanocrystals as well in the studies of the mechanism of the

(70) Tronc, E.; Ezzir, A.; Cherkaoui, R.; Chaneac, C.; Nogues, M.; Kachkachi, H.; Fiorani, D.; Testa, A. M.; Greneche, J. M.; Jolivet, J. P. *3rd EuroConference on Magnetic Properties of Fine Particles and Their Relevance to Materials Science*; Elsevier Science Bv: Barcelona, 1999; pp 63−79.
(71) Talapin, D. V.; Rogach, A. L.; Haase, M.; Weller, H. *J. Phys. Chem. B* **2001**, *105*, 12278–12285.
(72) Choi, J. S.; Jun, Y. W.; Yeon, S. I.; Kim, H. C.; Shin, J. S.; Cheon, J. *J. Am. Chem. Soc.* **2006**, *128*, 15982–15983.
(73) Melancon, M. P.; Lu, W.; Li, C. *MRS Bull.* **2009**, *34*, 415–421.

nucleation and growth of core/shell or dumbbell-like structures when the seed material contains the transition metals. This work was focused mostly on $CoPt_3$ NCs; however, there are many reasons to expect that similar trends will be observed in the case of other cobalt-based alloys as well as nickel- and copper-based NCs.

Acknowledgment. We acknowledge Prof. Horst Weller (University of Hamburg) and Thomas Möller (HASYLAB at DESY) for fruitful discussions. The work at the Center for Nanoscale Materials (ANL) was supported by the U.S Department of Energy under Contract No. DE-AC02-06CH11357. D.V.T. acknowledges the NSF CAREER under Award No. DMR-0847535. XPS measurements were supported by the German Science Foundation (DFG) within the framework of the SFB 508.

Supporting Information Available: EDX data; scheme of oxidation of luminol; spectrum and time decay of chemiluminesence; TGA data; FTIR data; calibration plot for $CoCl_2$ solutions; details of preparation of "inactive" $CoPt_3$ NCs; analysis of the different quenching factors of chemiluminensence; chemiluminsence on Co NCs, FC/ZFC on $CoPt_3$ NCs. This material is available free of charge via the Internet at http://pubs.acs.org.

JA102413K